STEM CELLS TRANSLATIONAL MEDICINE®

FETAL AND NEONATAL STEM CELLS

Early Intravenous Delivery of Human Brain Stromal Cells Modulates Systemic Inflammation and Leads to Vasoprotection in Traumatic Spinal Cord Injury

ANNA BADNER,[a,b] REAZ VAWDA,[a] ALEX LALIBERTE,[a,b] JAMES HONG,[a,b] MIRRIAM MIKHAIL,[a] ALEJANDRO JOSE,[a] RACHEL DRAGAS,[a,b] MICHAEL FEHLINGS[a,b,c]

Key Words. Mesenchymal stromal cells • Pericytes • Spinal cord injury • Vasoprotection • Interleukin-10

[a]Division of Genetics and Development, Toronto Western Research Institute, University Health Network, Toronto, Ontario, Canada; [b]Institute of Medical Science, University of Toronto, Toronto, Ontario, Canada; [c]Spinal Program, University Health Network, Toronto Western Hospital, Toronto, Ontario, Canada

Correspondence: Michael Fehlings, M.D., Ph.D., Institute of Medical Science, University of Toronto, Toronto Western Hospital, 399 Bathurst Street, Toronto, M5T 2S8 Ontario, Canada. Telephone: 416-603-5627; E-Mail: michael.fehlings@uhn.on.ca

Received October 14, 2015; accepted for publication March 7, 2016; published Online First on May 31, 2016.

1066-5099/2016/$20.00/0

http://dx.doi.org/10.5966/sctm.2015-0295

ABSTRACT

Spinal cord injury (SCI) is a life-threatening condition with multifaceted complications and limited treatment options. In SCI, the initial physical trauma is closely followed by a series of secondary events, including inflammation and blood spinal cord barrier (BSCB) disruption, which further exacerbate injury. This secondary pathology is partially mediated by the systemic immune response to trauma, in which cytokine production leads to the recruitment/activation of inflammatory cells. Because early intravenous delivery of mesenchymal stromal cells (MSCs) has been shown to mitigate inflammation in various models of neurologic disease, this study aimed to assess these effects in a rat model of SCI (C7-T1, 35-gram clip compression) using human brain-derived stromal cells. Quantitative polymerase chain reaction for a human-specific DNA sequence was used to assess cell biodistribution/clearance and confirmed that only a small proportion (approximately 0.001%–0.002%) of cells are delivered to the spinal cord, with the majority residing in the lung, liver, and spleen. Intriguingly, although cell populations drastically declined in all aforementioned organs, there remained a persistent population in the spleen at 7 days. Furthermore, the cell infusion significantly increased splenic and circulating levels of interleukin-10—a potent anti-inflammatory cytokine. Through this suppression of the systemic inflammatory response, the cells also reduced acute spinal cord BSCB permeability, hemorrhage, and lesion volume. These early effects further translated into enhanced functional recovery and tissue sparing 10 weeks after SCI. This work demonstrates an exciting therapeutic approach whereby a minimally invasive cell-transplantation procedure can effectively reduce secondary damage after SCI through systemic immunomodulation. STEM CELLS TRANSLATIONAL MEDICINE *2016;5:991–1003*

SIGNIFICANCE

Central nervous system pericytes (perivascular stromal cells) have recently gained significant attention within the scientific community. In addition to being recognized as major players in neurotrauma, pericytes have been discovered to share a common origin and potentially function with traditionally defined mesenchymal stromal cells (MSCs). Although there have been several in vitro comparisons, the in vivo therapeutic application of human brain-derived stromal cells has not been previously evaluated. This study demonstrates that these cells not only display a MSC phenotype in vitro but also have similar in vivo immunomodulatory effects after spinal cord injury that are more potent than those of non-central nervous system tissue-derived cells. Therefore, these cells are of great interest for therapeutic use in spinal cord injury.

INTRODUCTION

Despite improved mortality and advances in medical management, spinal cord injury (SCI) continues to result in severe sensorimotor deficits and a reduced quality of life with limited treatment options. As such, there is a need to advance our understanding of SCI pathophysiology and identify novel therapeutic strategies.

SCI occurs in two phases. The primary phase results from physical trauma, causing immediate structural disturbance and vascular damage [1]. The secondary phase includes inflammation and blood spinal cord barrier (BSCB) disruption, increasing tissue loss and, consequently, neurologic dysfunction. Secondary pathology is partially mediated by the systemic immune response, in which production of proteinases and inflammatory cytokines leads to recruitment and activation of peripheral leukocytes [2]. Although some immune cells may have proregenerative and/or neuroprotective functions [3], it is widely accepted

that therapies aimed at modulating (rather than suppressing) post-traumatic inflammation are an attractive treatment approach for acute SCI.

Mesenchymal stromal cells (MSCs) are under investigation for their immunomodulatory potential [4] in various models of central nervous system (CNS) disease [5]. In traumatic brain injury (TBI), early intravenous delivery of MSCs has been reported to mitigate the neuroinflammatory response by altering cytokine production [6–8], as well as recruitment of inflammatory cells [9–12]. These studies have also highlighted a role for cell interaction with peripheral immune organs in the inflammatory response [9, 13, 14], suggesting that local engraftment of transplanted MSCs is not necessary for therapeutic efficacy. Overall, encouraging preclinical results have led to two U.S. Food and Drug Administration-approved phase 1 safety trials using autologous bone marrow stromal cells for adult (clinicaltrials.gov identifier NCT01575470 [http://www.clinicaltrials.gov]) and pediatric (clinicaltrials.gov identifier NCT00254722) TBI [15]. It is hoped that these will successfully translate into clinically meaningful outcomes.

Mixed preclinical results have delayed clinical translation of MSCs for SCI. Variability among injury model, cell sources, administration, and transplantation timing has generated controversy [16] around cell therapy in SCI. Furthermore, the emphasis on cell survival and engraftment in SCI [17] and the relatively quick clearance of MSCs have led many to abandon their application. Systemic MSC transplantation in SCI has been investigated [10], but the relationship between transplanted cells and their effects on the spinal cord has been poorly defined, and the mechanisms of function are still unclear. To target this gap, this study profiles donor-cell biodistribution and clearance. Furthermore, this is the first study to identify a mechanism of systemic immunomodulation for cell-mediated effects within the spinal cord.

The ideal source of cells remains controversial. Evidence that MSCs can be found in the perivascular niche of most organs [18–20] has sparked debate regarding tissue-source differences in therapeutic potential of isolated cells. From an immunomodulatory perspective, MSCs of varying tissue origin have differential effects on the inhibition of T-cell proliferation [21], dendritic cell differentiation [22], and B-cell immunoglobulin production [23].

Although CNS perivascular stromal cells (pericytes) are known to be uniquely immunoregulatory [24], their effectiveness for cell therapy has remained unexplored. Given this, we evaluate whether CNS-derived stromal cells are better suited to treat SCI than cells derived from other sources. Hence, the present study not only addresses whether intravenously delivered stromal cells would alleviate the systemic inflammatory response, but also compares the efficacy of human fetal brain-derived stromal cells with those from the umbilical cord matrix—an alternative and ethical human fetal tissue source. Ultimately, we demonstrate that brain-derived pericytes not only display a MSC phenotype in vitro but also have similar in vivo immunomodulatory effects after SCI that lead to better functional recovery than those of non-CNS tissue-derived cells.

Materials and Methods

All animal experiments were approved by the animal care committee at the University Health Network (Toronto, Ontario, Canada) in compliance with the Canadian Council on Animal Care.

Cell Isolation and Culture

Human umbilical cord matrix cells (HUCMCs) were obtained from postpartum umbilical cord tissue (Chelsea and Westminster Hospital, London, U.K.). After the removal of veins and arteries, the Wharton's jelly (umbilical cord matrix) was diced and treated with collagenase I and II (1 mg/ml, Thermo Fisher Scientific, Oakwood Village, OH, https://www.thermofisher.com) for 2 hours at 37°C. The suspension was centrifuged at 2,000 rpm for 10 minutes before plating the cells on culture T175 flasks (Greiner Bio-One, Monroe, NC, https://www.gbo.com) in Minimum Essential Medium Eagle α Modification (α-MEM) with 10% fetal bovine serum (FBS) (Wisent Bioproducts, St. Bruno, Quebec, Canada, http://www.wisentbioproducts.com) and 0.1% gentamycin (Sigma-Aldrich, St. Louis, MO, http://www.sigmaaldrich.com). The human brain vascular pericytes (HBVPs; 1200, ScienCell Research Laboratories, Carlsbad, CA, https://www.sciencellonline.com) were cultured in pericyte medium (ScienCell Research Laboratories). The medium was replaced every 3 days, and the cells were grown to 80% confluence before passaging or cryogenic storage.

Immunophenotypic Cell Antigen Profiling

At passage 6–7, HUCMCs and HBVPs were cultured in glass chamber slides (Thermo Fisher Scientific) coated with fibronectin (Sigma-Aldrich). Once grown to 80%–90% confluence, the cells were fixed with 4% paraformaldehyde, permeabilized using 0.1% Triton X-100 in phosphate-buffered saline (PBS), blocked using 2% FBS (Wisent), and incubated overnight (4°C) with primary antibodies from the mesenchymal cell characterization kit (1:500; SCR067, EMD Millipore, Billerica, MA, http://www.millipore.com). Additional primary antibodies applied included mouse anti-human CD13 (1:500; C8589, Sigma-Aldrich), rabbit anti-α smooth muscle actin (1:300; AB124964, Abcam, Cambridge, MA, http://www.abcam.com), and rabbit anti-neural/glial antigen 2 (NG2) (1:200; AB5320, EMD Millipore). Slides were subsequently incubated with secondary antibody and with 4′,6-diamidino-2-phenylindole (DAPI; 1:1,000) as nuclear counterstain (2 hours, room temperature). Human bone marrow mesenchymal stem cells (HBM-MSCs; Lonza, Walkersville, MD, http://www.lonza.com) were used as a positive control.

Clip-Compression SCI and Tail Vein Infusion of Human Stromal Cells

Adult (10- to 11-week-old) female Wistar rats (250–300 g) were used (Charles River Laboratories, Wilmington, MA, http://www.criver.com). A combination of 0.05 mg/kg buprenorphine and 5 ml of saline was administered before surgical SCI. Under 1%–2% isoflurane anesthesia (delivered in a 1:1 mixture of O_2/N_2O), a laminectomy at the C7-T1 level was performed. A 1-minute, 35-g aneurysm clip-compression injury to the cord was then administered at C7. At 1 hour after SCI, 2.5 million passage-matched (6–7) stromal cells in 1 ml of Hanks' buffer/2 mM EDTA (HE) were slowly infused (200 μl/minute) via the tail vein. Postoperatively, buprenorphine, amoxicillin trihydrate/clavulanate potassium, and subcutaneous saline injections (0.9%, 5 ml) were administered. To reduce rejection, animals were immunesuppressed with daily subcutaneous cyclosporine injections (10 mg/kg). Animals were housed individually in standard cages (at 26°C–27°C), and their bladders were manually expressed.

In Vivo Very High-Resolution Ultrasound and Power Doppler Imaging

In vivo very high-resolution ultrasound (VHRUS) and power Doppler imaging were performed as previously described [25]. At 1, 3, and 7 days after injury, animals were anesthetized and placed on an imaging platform (Vevo Imaging Station, VisualSonics, Toronto, Ontario, Canada, http://www.visualsonics.com) with a custom-made stabilization frame. The injury was exposed through a midline incision and retraction of the paraspinal muscle layers. Ultrasound gel (scanning gel, Medi-Inn, Cameron, Ontario, Canada, http://info.cfimedical.com) was placed on the dura mater and scanned with the VHRUS probe (44 MHz, Vevo 770, VisualSonics) in three-dimensional (3D) power Doppler and B-modes. The 3D B-mode scans were analyzed by using ImageJ software as previously described [25], with minor modifications. Briefly, the bright pixels were delineated by three independent blinded observers within 19 central sagittal image slices and used to generate a reproducible lesion volume with the TrakEM2 plugin.

The function vascularity (active blood flow) was quantified by measuring the percent area of power Doppler signal [26] (color threshold positive pixels) in a standardized spinal cord region within the image slices. These values were normalized to time-matched shams and expressed as percentage of sham Doppler signal. The scan speed was 2.0 mm/second, and the wall filter was 2.5 mm/second.

Multiorgan DNA Extraction

Based on previous biodistribution profiles of intravenously infused MSCs [27], the heart, lung, liver, kidney, bladder, spleen, and 5-mm segment of injured spinal cord were collected after cell transplantation. The tissue samples were snap-frozen on dry ice after transcardial perfusion (with 250 ml of PBS) and ground into fine powder by using a mortar and pestle to produce a homogenous sample. Approximately 100 mg of the sample was collected for DNA extraction. A total of 1 ml of lysis buffer (0.1 M Tris [pH 8.0], 0.1 M NaCl, 5 mM EDTA, and 0.2% SDS) was added to each sample with 1 mg/ml of Proteinase K and incubated overnight (65°C). After incubation, the samples were spun down at 14,000 rpm for 10 minutes, and the supernatant was collected. A 1-volume equivalent of phenol:chloroform:isoamyl alcohol (25:24:1) was added to the supernatant, shaken, and allowed to settle (1 minute). The samples were again centrifuged at 12,000 rpm (5 minutes), and the aqueous phase was collected. A total of 4 μl of glycogen (5 μg/μl), 1 μl of ribonuclease, half-volume equivalent of 7.5 M ammonium acetate (pH 5.5), and 2.5-volume equivalent of 100% alcohol were added to the samples for overnight incubation at $-$20°C. Next, samples were centrifuged at 12,000 rpm for 30 minutes, and the pellet was collected. The pellet was washed with 70% alcohol three times, dried at room temperature (20 minutes), and resuspended in Tris-EDTA buffer. The amount of DNA was quantified with a NanoDrop spectrophotometer (ND-1000; Thermo Scientific).

Multiorgan Quantitative Real-Time Polymerase Chain Reaction for Human DNA Detection

Real-time polymerase chain reaction (PCR) was executed in an Applied Biosystems 7900HT Fast Real-Time PCR System (Applied Biosystems, Foster City, CA, http://www.appliedbiosystems.com) by using SyBr Green Mix (Thermo Fisher Scientific Life Sciences, Waltham, MA, http://www.thermofisher.com). A human-specific sequence of thymidine kinase was used to generate human primers (forward: 5′-ATGCTGATGGG-TAGGGTG-3′, reverse: 5′-TGAGTCAGGAGCCAGCGTATG-3′). Reactions were incubated at 95°C for 5 minutes, followed by 40 cycles at 95°C for 10 seconds and 63.5°C for 1 minute. Standard curves were generated by serial dilutions of human DNA in tissue-specific rodent DNA. Total DNA in the samples was assessed by using primers that amplified both the human and rodent gene for glyceraldehyde 3-phosphate dehydrogenase (forward: 5′-GCAAGAGAGCCCCTCAG-3′, reverse: 5′-TGTGAGGGAGATGCTCAGTC-3′). Because of detected changes in reaction efficiency between DNA extracted from varying tissue sources, each organ was run on an independent plate with standard curves generated from a matched tissue source.

Multiorgan Interleukin-10 Enzyme-Linked Immunosorbent Assay

Homogenous tissue samples from the DNA extraction experiments were used here. Protein was isolated from the spleen, lung, spinal cord, and liver (10 mg) by using 1$\times$ RIPA buffer (20-188; EMD Millipore) with the Halt protease and phosphatase inhibitor cocktail (78440; Thermo Fisher Scientific). Protein concentrations were quantified by using the microBCA protein assay kit (23235, Thermo Fisher Scientific). Once diluted to a protein concentration of 1 mg/mL, the samples were applied for the rat interleukin-10 (IL-10) enzyme-linked immunosorbent assay (ELISA) kit (AB100765; Abcam) per the manufacturer's instructions. Absorbance was read at 450 nm (Wallac 1420 VICTOR2; PerkinElmer, Waltham, MA, http://www.perkinelmer.com).

Prelabeling Cells (CellTracker Dye) and Multiorgan Confocal Imaging

A concentration of 5 μM CellTracker Red CMTPX dye (C34552; Thermo Fisher Scientific) was used to label cells before infusion. The spinal cord, lungs, and spleen were collected after transcardial perfusion with 180 ml of PBS and 60 ml of 4% paraformaldehyde (PFA) at 1 day after cell infusion. The tissue was postfixed for 1 day, cryoprotected in 30% sucrose (in PBS), embedded in optimal cutting temperate (OCT) medium (Thermo Fisher Scientific), and cut into 30-μm-thick cross-sections. These tissue sections were additionally stained with rat endothelial cell antigen 1 (RECA-1) and DAPI (described in immunohistochemistry methods). Images were taken with the Nikon C2+ confocal laser microscope (Nikon, Tokyo, Japan, http://www.nikon.com) at $\times$60.

Tissue Processing and Immunohistochemistry

Animals were transcardially perfused with 180 ml of PBS and another 60 ml of chilled 4% PFA. The tissue was postfixed for 1 day and then cryoprotected in 30% sucrose before embedding in OCT medium (Thermo Scientific). The 1.5-cm-length spinal cord segments were cut into 30-μm transverse sections. For immunohistochemistry, the slides were dried and rinsed with 1$\times$ PBS and blocked (blocking solution; 2% FBS and 0.1% Triton X in 1$\times$ PBS) for 1 hour at room temperature. Primary antibodies for anti-mouse RECA-1 (1:250; AbD Serotec, Kidlington, U.K., https://www.abdserotec.com) and fluorescein isothiocyanate-conjugated polymorphonuclear leukocytes (1:100; CLFAD51140, Cedarlane Laboratories, Burlington, Ontario, Canada, https://www.cedarlanelabs.com) were diluted in blocking solution and

left overnight at 4°C. After three washes (15 minutes), secondary antibodies were applied as necessary with DAPI (1:1,000).

Quantitative Analysis of Immunohistochemistry: Blood Vessel Density

Images were taken at ×20 on the Zeiss Axioplan 2 fluorescence microscope (Zeiss, Stuttgart, Germany, http://www.zeiss.com). ImageJ software was used to manually count all RECA1+ blood vessels on three randomly selected view fields (ventral horn, dorsal horn, and lateral column) for each cross-section in a blinded manner as previously described [28]. The rostro-caudal sampling was evenly distributed (at 500-nm intervals) along 1 mm of the spinal cord centered on the injury epicenter. The vessel count values were pooled, and data were expressed as the percentage of time-matched sham values. Separate results are presented for gray matter and white matter.

Evans Blue Assay for BSCB Integrity

Evans Blue (EB) extravasation was quantified through spectrophotometry as previously described [29] with minor modifications. Briefly, 1 ml of 2% EB (in PBS) was infused via the femoral vein and allowed to circulate for 30 minutes before transcardial perfusion with 250 ml of PBS. A total of 5 mm of injured spinal cord tissue was removed and weighed. The tissue was homogenized (pulse sonication on ice, 1 minute) in dimethylformamide (D4551; Sigma-Aldrich), incubated at 50°C for 72 hours, and centrifuged at 18,000 rpm (centrifuge 5417, Eppendorf, Hauppauge, NY, https://www.eppendorf.com). The supernatant was transferred into a 96-well glass plate (Zeiss), and absorbance was measured at 620 nm (Wallac 1420 VICTOR2; PerkinElmer). EB concentration was calculated based on a standard curve, and values were normalized to tissue weight (grams).

Drabkin's Assay for Intraparenchymal Hemorrhage

Intraspinal hemoglobin was quantified as previously described [30]. After transcardial perfusion with 250 ml of PBS, 5 mm of the injured spinal cord was removed and weighed. Samples were homogenized in 100 μl of distilled water on ice for approximately 1 minute. The homogenates were subsequently spun down at 13,000 rpm for 15 minute, and supernatant was collected. A total of 20 μl of supernatant was added to 80 μl of Drabkin's reagent (Drabkin's Reagent powder [D5941]; Sigma-Aldrich] in 1,000 ml of distilled H_2O and 0.5 ml of 30% Brij 35 Solution) in a clear 96-well plate and incubated for 15 minute. Absorbance was read at 560 nm (Wallac 1420 VICTOR2; PerkinElmer), normalized by weight, and concentration was calculated based on a linear bovine blood hemoglobin (H2500; Sigma-Aldrich) standard curve.

Cytokine Array for Rodent Plasma Analysis

Blood was collected into EDTA-coated Vacutainer tubes (K2 EDTA Plus Blood Collection Tubes, BD Biosciences, San Jose, CA, http://www.bdbiosciences.com) via cardiac puncture before perfusion. Blood samples were immediately centrifuged at 3,000 rpm (centrifuge 5810R, Eppendorf) for 10 minutes (4°C), and the plasma was collected. The rat cytokine R&D ELISA Proteome Profiler array (ARY008, R&D Systems Inc., Minneapolis, MN, https://www.rndsystems.com) was used as per manufacturer's instructions with minor modifications. Briefly, IRDye 800CW Streptavidin (926-32230, LI-COR, Lincoln, NE, https://www.licor.com) was used at a 1:2,000 dilution (30 minutes, room temperature) as replacement for the kit's Streptavidin-horseradish peroxidase to increase detection sensitivity. Proteome array membranes were scanned on an Odyssey Imager CLx (LI-COR). The scans were quantified by using a semiautomated ImageJ macro, in which the 700 channel was applied to generate detection spot coordinates for mean gray value measurements on the 800 channel. These values were normalized to time-matched controls and expressed as percentage of sham signal.

Lesion Morphometry (10 Weeks After SCI)

Cross-sectional (30 μm) serial sections (n = 4 per group) were stained with Luxol fast blue (LFB) and hematoxylin and eosin (H&E) as previously described [31]. Sections were systematically sampled at every 300 μm over 5,400 μm, and unbiased measurements were made with a Cavalieri probe using Stereo Investigator (MBF Bioscience, Williston, VT, http://www.mbfbioscience.com) for lesional tissue, gray matter, and white matter percent area.

Long-Term Neurobehavioral Assessment (10 Weeks after SCI)

All neurobehavioral assessments were performed weekly for 10 weeks after SCI (vehicle, n = 11; HUCMC, n = 11; HVBPs, n = 10) by examiners blinded to experimental group. Forelimb motor function was assessed with a grip strength meter (SDI Grip Strength System, model DFM-10; San Diego Instruments, San Diego, CA, http://www.sandiegoinstruments.com) as previously described [32].

Whole-body limb function and trunk stability was evaluated with the inclined plane test [33]. Rats were placed on a horizontal plane and the incline angle was incrementally raised until they were no longer able to maintain their position. Hind-limb locomotion was assessed by using the 22-point (0–21) Basso, Beattie, and Bresnahan (BBB) Locomotor Rating Scale as previously described [34].

Statistical Analysis

Quantitative data are expressed as the mean ± SEM. Differences among groups were assessed by one- and two-way analysis of variance (ANOVA) with Dunnett's (for profiling data) or Tukey's (for cell comparisons) post hoc tests (statistically significant at $p \leq .05$). Data were analyzed with GraphPad Prism (GraphPad Software Inc., La Jolla, CA, USA, http://www.graphpad.com).

RESULTS

Immunophenotypic Cell Antigen Profile

HUCMCs and HBVPs were screened for mesenchymal (STRO-1, CD44, CD105, and CD146) and pericyte (CD13, NG2, and α-smooth muscle actin [α-SMA]) markers at passage 6–7 and 80%–90% confluence (Fig. 1). Commercially available HBM-MSCs were used as a positive staining control. Although the marker expression was similar between HUCMCs and HBVPs, HUCMCs did not express α-SMA (Fig. 1).

Biodistribution and Clearance of Intravenously Delivered Stromal Cells

After cell infusion, the temporal biodistribution of transplanted cells was assessed with quantitative reverse-transcription

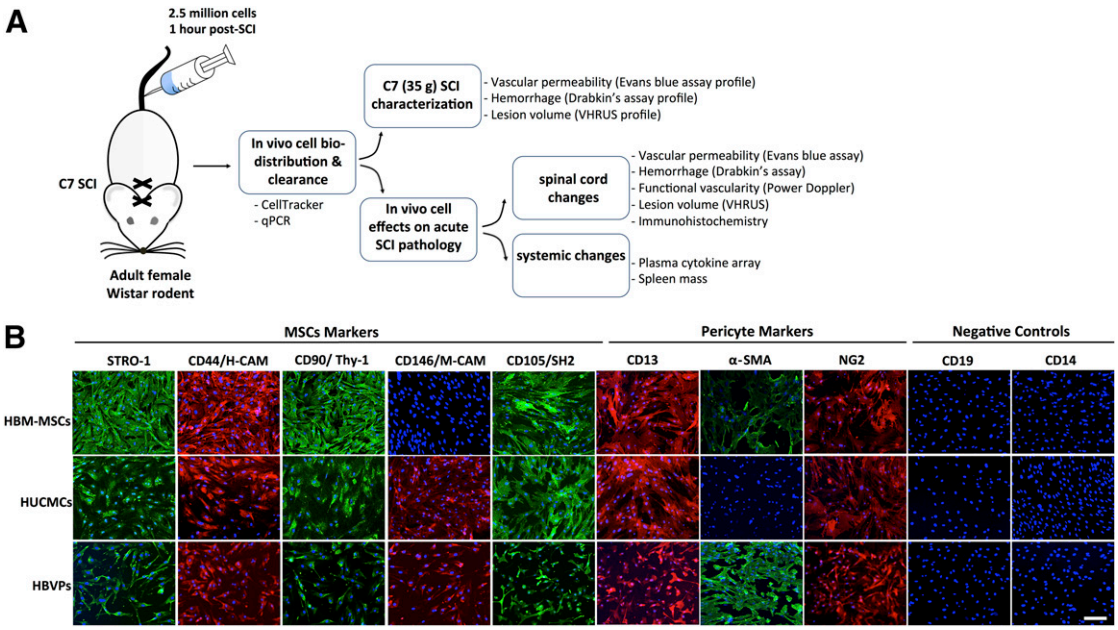

Figure 1. Experimental approach and stromal cell immunophenotypic cell surface antigen expression profile. **(A):** Study design illustrating the experiments and protocols applied. In short, adult female Wistar rats (~250 g) received a C7 35-g clip-compression injury. At 1 hour after SCI, 2.5×10^6 stromal cells (HUCMCs or HBVPs) were infused via the tail vein, and their biodistribution/clearance was assessed with quantitative reverse-transcription polymerase chain reaction and CellTracker confocal imaging. Spinal cord changes in vascular permeability, hemorrhage, and lesion were initially profiled to identify relevant time points for study of cell effects. **(B):** HUCMC and HBVP surface antigen expression was assessed with immunocytochemistry. Representative images were taken at ×10 with the Zeiss LSM 510 META confocal microscope. Scale bar = 150 μm. Abbreviations: α-SMA, α-smooth muscle actin; H-CAM, homing-associated cell adhesion molecule; HBM-MSCs, human bone marrow mesenchymal stem cells; HBVPs, human brain vascular pericytes; HUCMCs, human umbilical cord matrix cells; M-CAM, melanoma cell adhesion molecule; MSCs, mesenchymal stem cells; qPCR, quantitative polymerase chain reaction; SCI, spinal cord injury; VHRUS, very high-resolution ultrasound.

polymerase chain reaction (qRT-PCR) for a human-specific sequence (Fig. 2) in spinal cord as well as the heart, lungs, liver, kidneys, spleen, and bladder. As mentioned, real-time PCRs were run independently for each organ with tissue-specific standard curves. No human DNA was detected in the heart and bladder, with only trace amounts in the kidneys. At 1 day after SCI, the majority of human DNA signal (converted to approximate number of human cells) [27] was found in the lungs followed by the liver. There were 355.3 ± 74.8 HUCMCs and 180 ± 100.1 HBVPs per million rat cells in the lungs, compared with 35.9 ± 5.9 HUCMCs and 17.7 ± 2.7 HBVPs per million rat cells in the liver. Although most organs had no detectable human DNA by 7 days after SCI, there were 175.3 ± 30.5 HUCMCs and 298.2 ± 65.5 HBVPs per million rat cells in the spleen. To validate the quantitative polymerase chain reaction signal, HUCMCs were labeled with CellTracker Red CMTPX dye before infusion after SCI, and the tissue was collected for immunohistochemistry 1 day after SCI. Many of these were detected as clusters within blood vessels (RECA-1+ cells) of the lungs (Fig. 2E). Within the liver and spleen, there were significantly fewer cells present, and they were dispersed among the tissue (Fig. 2F, 2G).

Circulating Cytokine Changes After Intravenous Stromal Cell Infusion After SCI

Of 29 cytokines evaluated with the R&D ELISA Proteome Profiler array (Fig. 3), only plasma IL-10 had significantly increased levels after HUCMC (0.42- ± 0.15-fold change, one-way ANOVA, Tukey's post hoc, p = .016) and HBVP (0.44- ± 0.06-fold change, one-way ANOVA, Tukey's post hoc, p = .013) infusion (Fig. 3). Although only lipopolysaccharide-induced CXC chemokine (LIX; CXCL5) was significantly affected by infusion of HBVPs (one-way ANOVA, p = .04), thymus chemokine/CXCL7 and regulated on activation, normal T-cell expressed and secreted (RANTES)/CCL5 showed trends toward increased (one-way ANOVA, p = .06) and decreased (one-way ANOVA, p = .06) levels between the vehicle control and HBVPs, respectively. Tissue inhibitor of matrix metalloproteinase 1 (TIMP-1) levels (one-way ANOVA, p = .07) showed an increasing trend after HUCMC (0.12- ± 0.01-fold change) and HBVPs (0.14- ± 0.014-fold change) infusion compared with the vehicle control (0.05- ± 0.04-fold change).

To identify the tissue source of IL-10 synthesis and release resulting from stromal cell infusion, IL-10 changes were evaluated in the organs retaining transplanted cells (Fig. 3F). Only the spleen had a significant rise in IL-10 after HUCMC (one-way ANOVA, Tukey's post hoc, p = .03) and HBVP (one-way ANOVA, Tukey's post hoc, p = .01) infusion. There was also a trend toward (one-way ANOVA, p = .068) preservation of spleen mass 3 days after SCI (Fig. 3G).

Stromal Cells Reduce BSCB Permeability, Hemorrhage, and Acute Lesion Volume

To identify the timing of secondary vascular pathology, BSCB permeability, hemorrhage, and lesion volume were profiled (Figs. 4 and 5). EB extravasation and hemorrhaging in the spinal cord peaked at 1 day after SCI, with 25.25 ± 2.34 μg/ml EB per gram of tissue (one-way ANOVA, Dunnett's post hoc, $p < .0001$) and 559.7 ± 40.9 μl of blood per gram of wet tissue (one-way ANOVA,

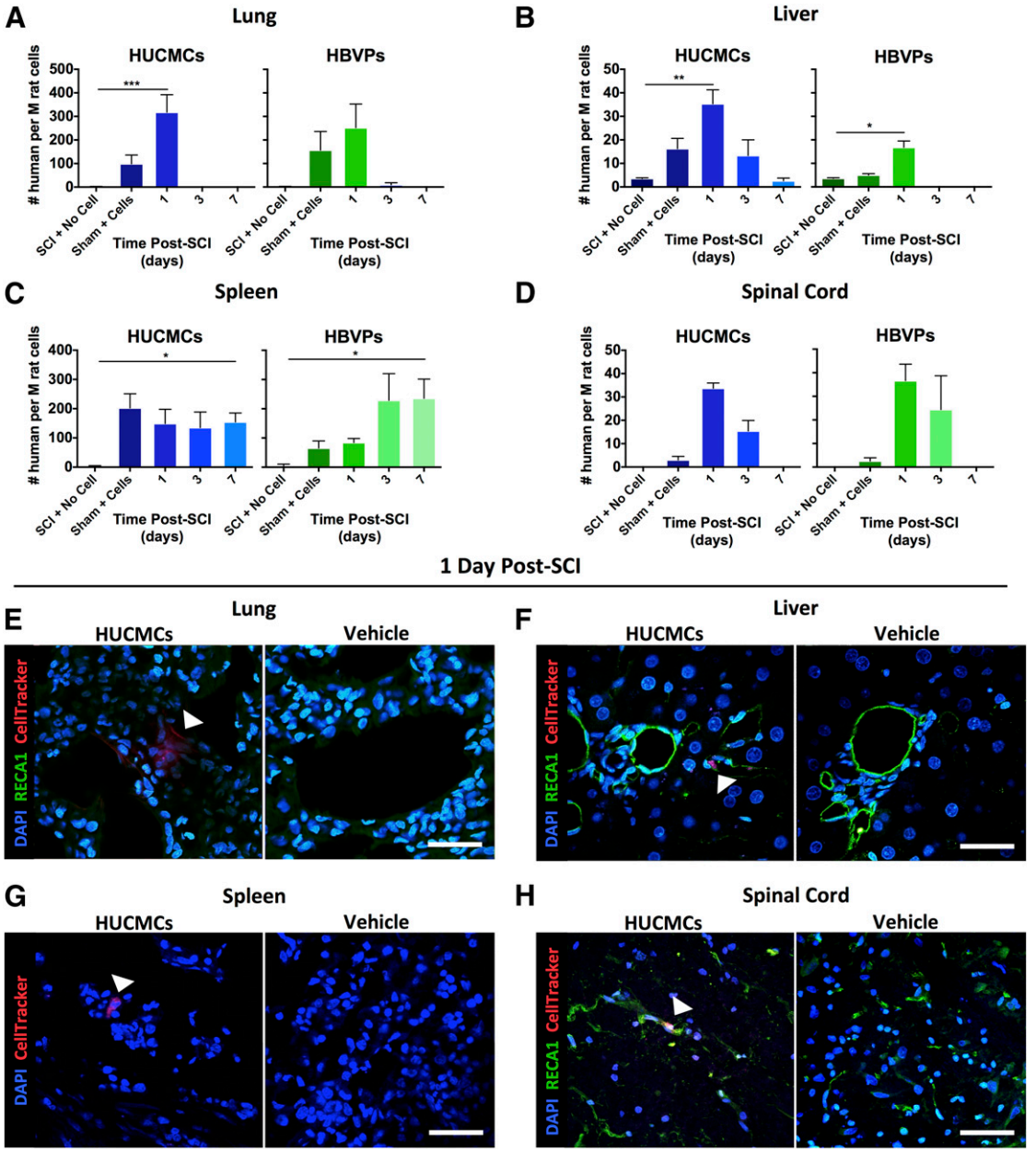

Figure 2. Temporal human stromal cell bio-distribution after intravenous delivery following SCI reveals rapid cell clearance. **(A–D):** Quantitative reverse-transcription polymerase chain reaction for a human-specific sequence of DNA (thymidine kinase) was used to assess temporal cell (HUCMC and HBVP) clearance in the lungs **(A)**, liver **(B)**, spleen **(C)**, and spinal cord **(D)**. Data were converted to number of human cells (per million rat cells) and are expressed as mean ± SEM. **(E–H):** HUCMCs were also labeled with CellTracker dye before infusion for confocal imaging (×60, Nikon C2+ microscope) of their distribution in the lungs **(E)**, liver **(F)**, spleen **(G)**, and spinal cord white matter **(H)** at 1 day (24 hours) after SCI. Arrows indicate CellTracker signal, One-way analysis of variance (Dunnett's multiple comparison). *, $p \leq .05$; **, $p \leq .01$; ***, $p \leq .001$; ****, $p \leq .0001$. Scale bar = 50 μm. Abbreviations: DAPI, 4′,6-diamidino-2-phenylindole; HBVPs, human brain vascular pericytes; HUCMCs, human umbilical cord matrix cells; M, million; RECA1, rat endothelial cell antigen 1; SCI, spinal cord injury.

Dunnett's post hoc, $p < .0001$), respectively. The lesion volume, as measured by VHRUS, reached maximum at 2 days after SCI (26.5 ± 2.1 mm^3), only slightly larger than at 1 day after SCI (20.7 ± 1.0 mm^3). Based on the profiling results, the effects of intravenous stromal cell delivery on vascular pathology were assessed at 1 day after SCI. The vehicle control (29.41 ± 1.38 34 μg/ml EB per gram of wet tissue) had significantly ($p < .01$) more vascular permeability than HUCMC-infused (24.58 ± 0.87 μg/ml EB per gram of wet tissue) or HBVP-infused (23.91 μg/ml EB per gram of wet tissue) animals. Similarly, cell infusion (338.5 ± 24.2 and 318.7 ± 20.6 μl of blood per gram of wet tissue for HUCMC and HBVPs, respectively) reduced ($p < .01$) the amount of hemorrhaging in the spinal cord relative to the vehicle control (493.1 ± 18.0 μl of blood per gram of wet tissue).

Changes in lesion volume were evaluated via VHRUS at 1, 3, and 7 days after SCI (Fig. 5). Although there was a significant difference between cell-infused and vehicle control animals at each time point, the most striking effects were found at 3 days. The

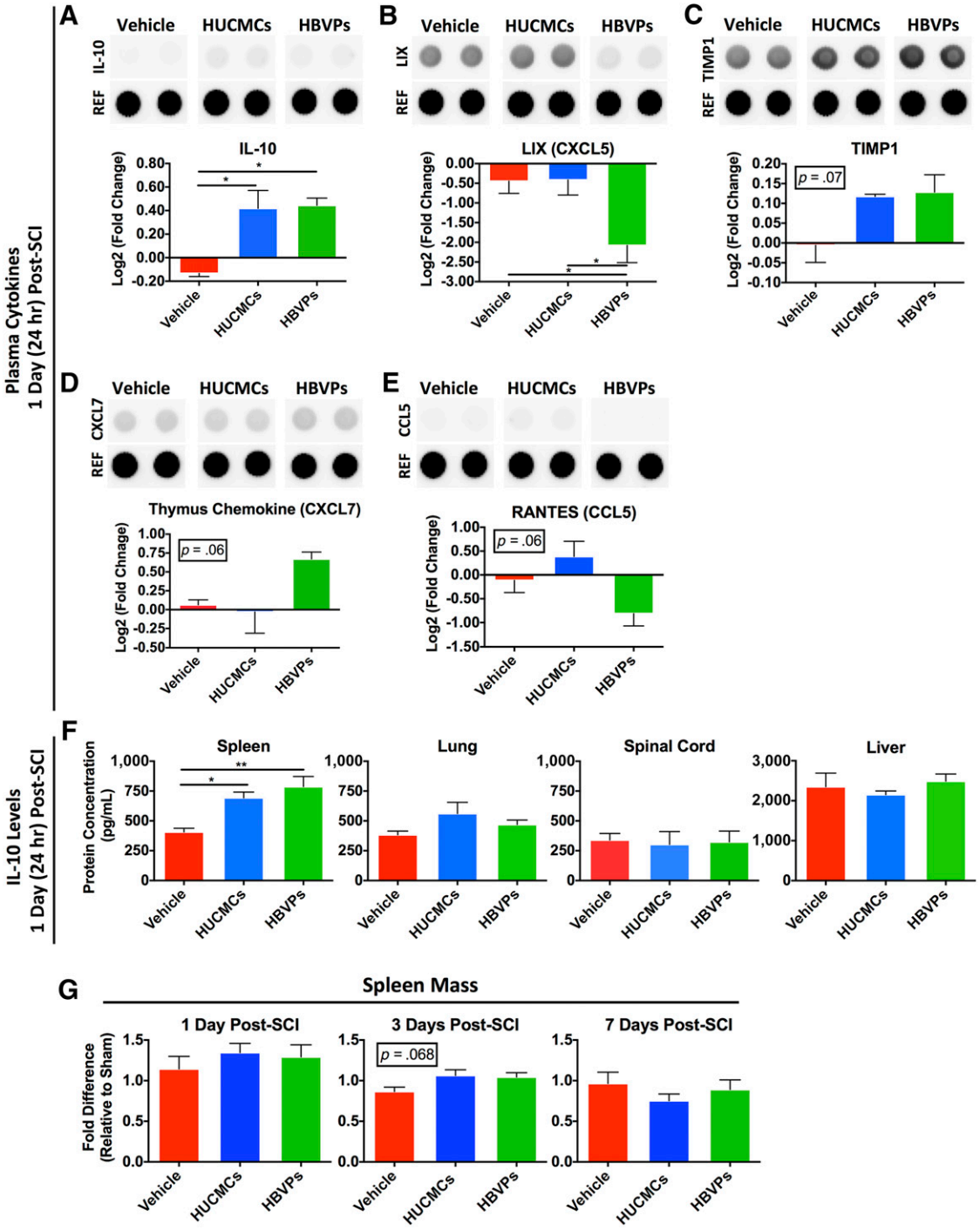

Figure 3. Stromal cell infusion raises rodent circulating and splenic IL-10 levels at 1 day (24 hours) after SCI. Because very few cells were found in the spinal cord after intravenous infusion, we sought to characterize the systemic response. Rodent plasma cytokines changes were assessed with the R&D enzyme-linked immunosorbent assay (ELISA) Proteome Profiler array (ARY008), which compares the relative levels of 29 cytokines. The protein levels were normalized to time-matched sham (laminectomy only) controls, $n = 3$. **(A–D):** Differences between the experimental groups are shown for IL-10 **(A)**, LIX/CXCL5 **(B)**, TIMP1 **(C)**, thymus chemokine/CXCL7 **(D)**, and RANTES/CCL5 **(E)**. Only IL-10 levels were significantly higher after infusion of both stromal cell types. **(F):** Therefore, to identify the tissue source of IL-10 synthesis and release into the circulation after stromal cell infusion, tissue lysate ($n = 3$–4) from the spleen, lungs, spinal cord, and liver was quantified with an Abcam rodent ELISA kit (AB100765). There was only a significant rise in IL-10 levels within the spleen after stromal cell infusion. **(G):** The spleen mass (shown as fold difference relative to time-matched laminectomy only controls) was also evaluated at 1, 3, and 7 days after SCI. One-way analysis of variance (Tukey's multiple comparison). $*$, $p \leq .05$; $**$, $p \leq .01$. Abbreviations: CCL5, chemokine (C-C motif) ligand 5; CXCL5, C-X-C motif chemokine 5; HBVPs, human brain vascular pericytes; HUCMCs, human umbilical cord matrix cells; IL-10, interleukin 10; LIX, lipopolysaccharide-induced CXC chemokine; RANTES, regulated on activation, normal T cell expressed and secreted; REF, reference control; TIMP1, tissue inhibitor of matrix metalloproteinase 1.

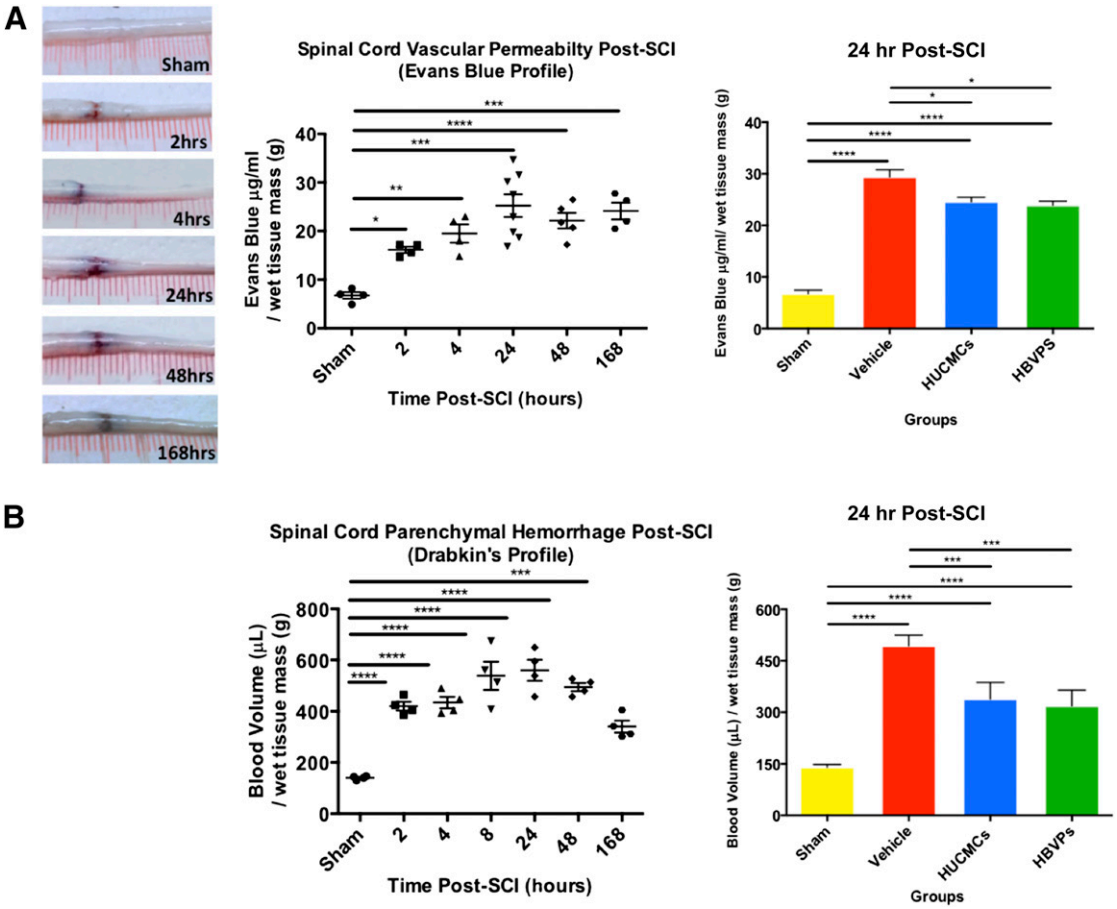

Figure 4. Stromal cell infusion reduces blood spinal cord barrier permeability (Evans Blue extravasation) and hemorrhage (Drabkins' assay) after SCI. **(A):** Representative images of C7 (35 g) SCI Evans Blue extravasation and concentration (μg/mL) in spinal cord over time. **(B):** The Drabkins' assay was applied to quantify the spinal cord hemorrhaging (blood volume) over time and after stromal cell infusion at 24 hours after SCI. Data are expressed as mean ± SEM. One-way analysis of variance (Dunnett's post hoc for temporal profiles, Tukey's post hoc for cell comparison). *, $p \leq .05$; **, $p \leq .01$; ***, $p \leq .001$; ****, $p \leq .0001$. Abbreviations: HBVPs, human brain vascular pericytes; HUCMCs, human umbilical cord matrix cells; SCI, spinal cord injury.

vehicle control had a lesion volume of 31.5 ± 0.7 mm^3, whereas the HUCMC- and HBVP-infused animals had volumes of 22.9 ± 1.2 and 24.9 ± 1.6 mm^3, respectively.

Stromal Cells Improve Functional Vascularity With No Effect on Blood Vessel Density After SCI

After the significant effects of intravenous stromal cell infusion on vascular integrity, vessel function was evaluated by using 3D power Doppler imaging with VHRUS at 1, 3, and 7 days after SCI (Fig. 6). Consistent with previous results, vascular function was significantly (one-way ANOVA, Tukey's post hoc, $p = .014$) preserved with HBVPs (79.4 ± 8.3% of sham signal) compared with the vehicle control (50.5 ± 4.1% of sham signal) at 1 day. Although the effect of HUCMCs did not reach statistical significance (one-way ANOVA, Tukey's post hoc, $p = .09$), the mean power Doppler functional vascularity (72.8 ± 8.4% of sham signal) was considerably greater than in controls. Because there was natural recovery of functional vascularity at 3 and 7 days after SCI, cell effects were lost at these time points.

To further assess whether detected vascular differences were a result of anatomical changes after stromal cell infusion, the number of vessels was quantified with immunohistochemistry for RECA-1. Although there was a decrease in the number of vessels at 1 day after injury compared with laminectomy-only controls, there was no difference in gray or white matter vessel counts between the groups (Fig. 6).

Stromal Cell Infusion Enhances Functional Recovery and Tissue Sparing

We examined long-term functional recovery after stromal cell infusion using standardized behavioral tests (Fig. 7B–7D). Both cell types significantly (two-way ANOVA, $p < .0001$) enhanced the restoration of grip strength (Fig. 7B). As early as 3 weeks after SCI, HUCMC (970.8 ± 73.5 g) and HBVP-treated (1,225.2 ± 32.8 g) animals had significantly (Tukey's post hoc test, $p < .05$) improved grip strength compared with vehicle controls (753.6 ± 38.5 g). Interestingly, HBVPs uniquely improved (two-way ANOVA, $p < .0001$) whole-body limb coordination and trunk stability, as measured by the inclined plane test (Fig. 7C). HBVPs also improved hind-limb locomotion, assessed with the BBB scale (Fig. 7D). At 10 weeks after SCI, HBVP-treated animals obtained an average BBB score of 11.35 ± 0.44 compared with 9.27 ± 0.54 for vehicle controls ($p < .05$).

Histomorphometric analysis with LFB- and H&E-stained sections was used to quantify the lesion and gray and white matter

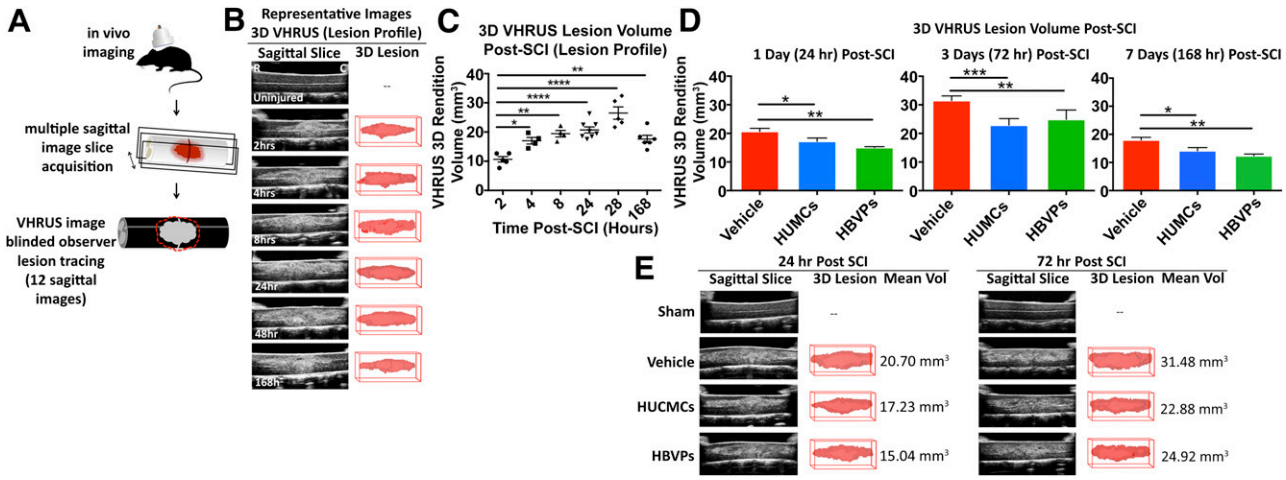

Figure 5. Stromal cell infusion reduces the acute lesion volume. **(A):** In vivo very high-resolution ultrasound imaging in B-Mode (11 × 7 mm) was used to quantify the acute lesion volume. **(B, C):** Representative images of the C7 (35 g) SCI lesion **(B)** and quantified volumes **(C)** are shown over time. **(D):** HUCMCs as well as HBVPs reduced the SCI lesion volume at 1, 3, and 7 days. Data are expressed as mean ± SEM. **(E):** Representative images of the VHRUS scans and 3D lesion reconstructions are shown for all the experimental groups. One-way analysis of variance (Dunnett's for temporal profiles, Tukey's post hoc for cell comparison). *, $p \leq .05$; **, $p \leq .01$; ***, $p \leq .001$; ****, $p \leq .0001$. Abbreviations: 3D, three-dimensional; HBVPs, human brain vascular pericytes; HUCMCs, human umbilical cord matrix cells; SCI, spinal cord injury; VHRUS, very high-resolution ultrasound; Vol, volume.

tissue changes at 10 weeks after SCI (Fig. 7E, 7F). Reduced lesional tissue and increased white matter sparing was observed 300 μm rostro-caudal and 600 μm rostral to the injury epicenter in cell-treated animals (two-way ANOVA, $p < .05$). Preservation of gray matter was observed rostral to the injury (1,200–1,800 μm). Because our injury model spans the boundary between cervical and thoracic levels, it is interesting that gray matter sparing was restricted to the more vascularized cervical region.

Discussion

Here, we demonstrate that early intravenous infusion of human stromal cells for SCI has protective effects on blood vessels. Despite limited engraftment and rapid clearance of cells, the infusion increased levels of circulating and splenic IL-10. Moreover, cell transplantation reduced EB extravasation and hemorrhaging within the acutely injured spinal cord. Although there were no changes in the number of perilesional blood vessels, HBVPs improved functional vascularity and plasma LIX levels. Furthermore, HBVPs enhanced recovery of whole-body coordination and trunk stability, as well as locomotion. Both cell types led to similar improvements in grip strength. These results provide evidence that stromal cells may mitigate secondary vascular pathology through modulation of the systemic inflammatory response. Furthermore, differences between results from HUCMCs and HBVPs indicate cell source-dependent variations in immunomodulatory potential. Although pericytes have been investigated therapeutically in heart disease [35, 36] and retinal vasculopathy [37], this is the first assessment of human brain-derived pericytes for SCI. In addition to being the first study to examine any stromal cell source in a cervical injury, it is also one of the only studies to address the knowledge gap regarding low cell engraftment at the lesion, quick cell clearance, and localized spinal cord effects.

Investigation of high thoracic/cervical-level injuries is important for clinical translation. Because high-level injuries disrupt the innervation of lymphoid tissue [38], they lead to altered immune function and an inflammatory response distinct from the lower-level injuries most commonly studied [39–41]. Splenic innervation, in particular, has been shown to regulate cytokine production/release [42], as well as leukocyte activation [43] during inflammation. Furthermore, because the spleen has been previously implicated as a site of MSC function [9, 44], we were interested in splenic cell localization (Fig. 2) and effects on spleen atrophy (Fig. 3). In TBI, Walker et al. demonstrated that a primitive form of BM-MSCs was found in the spleen within 6 hours of intravenous injection [9]. They further showed that cell infusion reduced spleen atrophy and increased CD4+ T-cell proliferation as well as IL-4 and IL-10 production in splenocytes [9]. Because reductions in spleen mass have been attributed to the release of spleen-derived immune cells [45], these results, combined with the production of splenic anti-inflammatory cytokines, support the conclusion that transplanted MSCs can modulate the immunologic response. Interestingly, here, splenic human DNA signal peaked at 7 days after SCI (for both cell types), and there was a trend toward spleen mass preservation after cell infusion (at 3 days after SCI; Fig. 3). Furthermore, although we found CellTracker-labeled HUCMCs in the spleen 1 day after SCI (Fig. 2), it is unclear whether the cells gradually accumulate in the spleen to peak at 7 days. Therefore, despite ample evidence of splenic involvement in SCI and MSC mechanisms independently, their exact relationship remains unclear and will be the subject of future studies.

Intravenous Stromal Cells for Vascular Protection

Consistent with our EB extravasation results, the literature reports improvements in acute vascular integrity after CNS trauma with systemic infusion of rodent [10, 46–48] and human stromal cells [6, 8, 9]. Reductions in lesion volume [49], especially in the early phases of injury [50], have also been described. Although multiple mechanisms are likely implicated, the two best-described molecular mediators to date have been TIMP-3 [6]

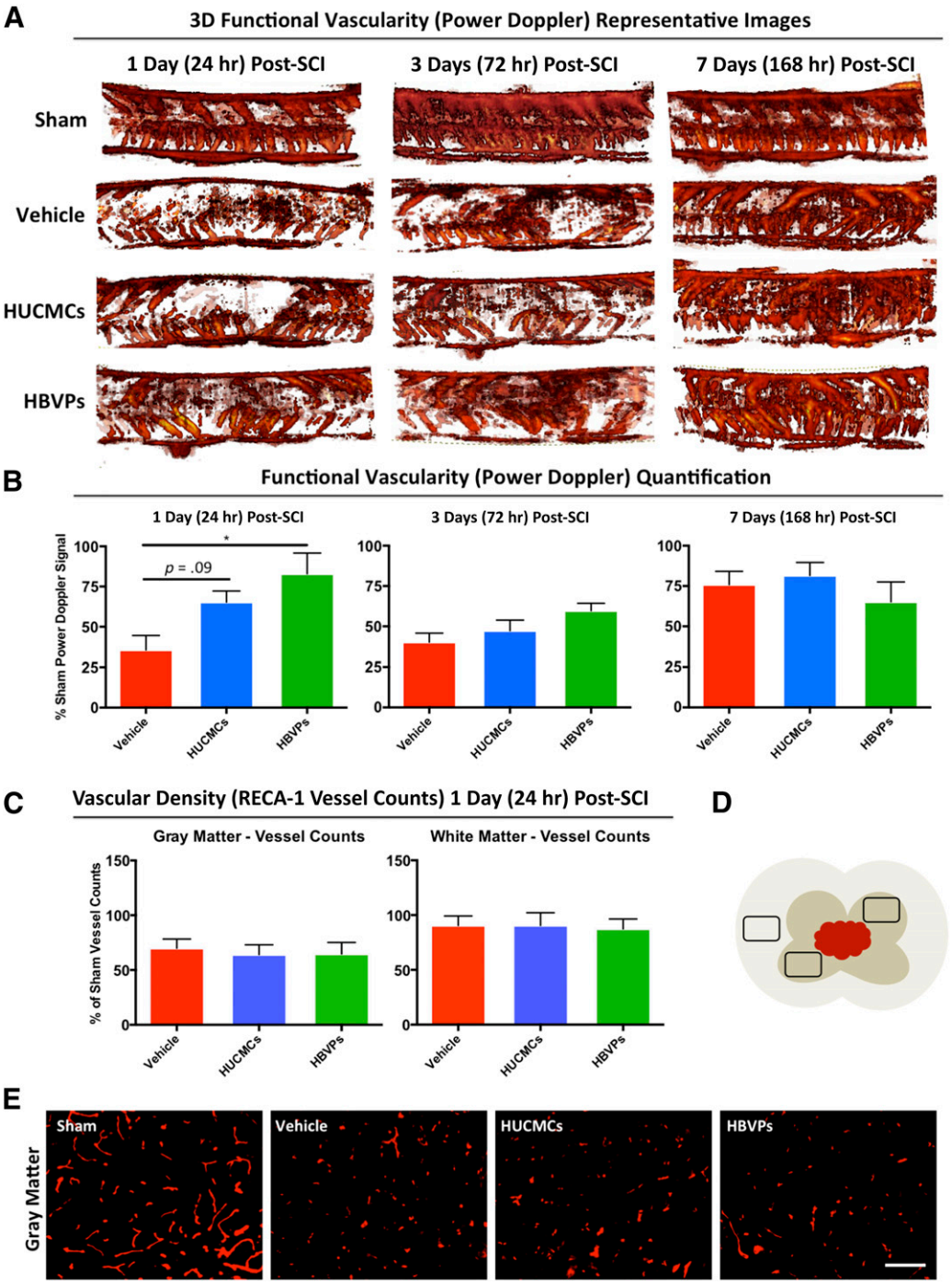

Figure 6. HBVP infusion improves acute functional vascularity (3D power Doppler imaging) at 24 hours after SCI, with no detectable effect on blood vessel density (RECA-1 counts). Very high-resolution ultrasound (VHRUS) imaging in power Doppler mode was applied to quantify functional vascularity (active blood flow) within the injured spinal cord. **(A):** Representative 3D power Doppler signal image stacks (of the 19 central sagittal slices) are shown for all the experimental groups at 1, 3, and 7 days after SCI. Increases in Doppler signal (shown in red) correspond to increased vascularity. The color threshold positive pixels (defined as power Doppler signal) were quantified in a standardized spinal cord region as a measure of functional vascularity. **(B):** The quantified signal was normalized to time-matched sham (laminectomy only) and is expressed as a percentage of sham signals for all the experimental groups at 1, 3, and 7 days after SCI. **(C):** Vascular density (obtained from vessel counts) was normalized to time-matched sham controls for the same region of the spinal cord and are expressed as the percentage of sham vessels. **(D):** A schematic of cross-sectional spinal cord highlights the preselected areas for vessel quantification. The dorsal and ventral horns were preselected for gray matter assessment, whereas the lateral white matter column was applied for white matter counts over a distance of 1 mm centered on the injury epicenter. Data are expressed as mean ± SEM, $n = 4$ per group. One-way analysis of variance (Tukey's multiple comparison). $*, p \leq .05$. **(E):** Representative images taken at ×20 are shown for all experimental groups. Abbreviations: HBVPs, human brain vascular pericytes; HUCMCs, human umbilical cord matrix cells; RECA-1, rat endothelial cell antigen 1; SCI, spinal cord injury.

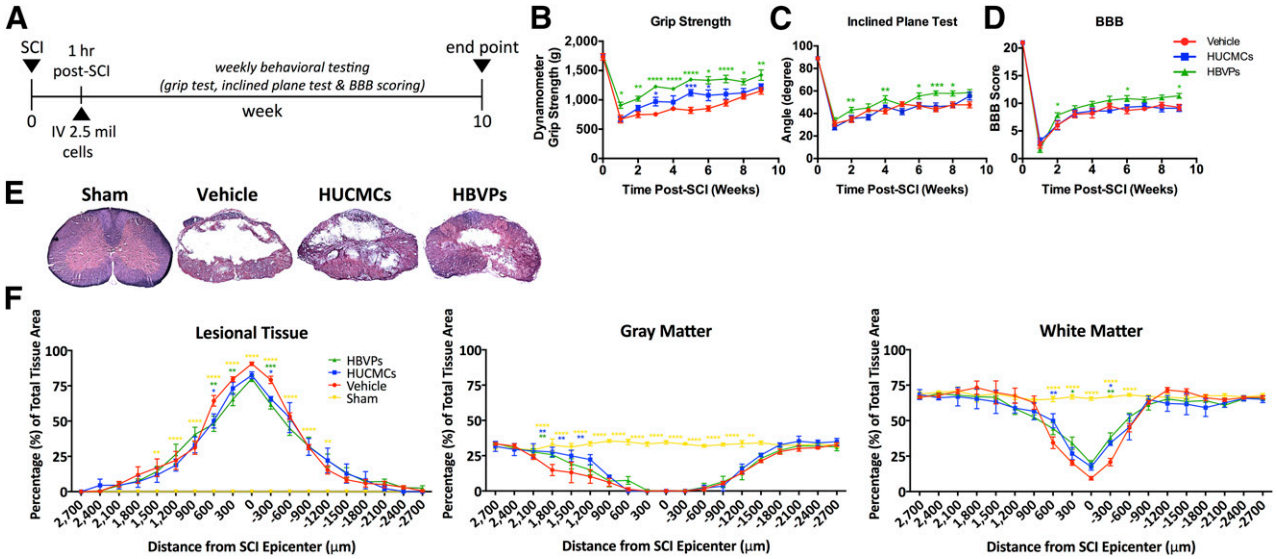

Figure 7. Early intravenous stromal cell infusion enhances functional recovery and tissue sparing. **(A):** Long-term experimental design and timeline. In short, weekly standardized behavioral testing was applied for 10 weeks after SCI and cell infusion (vehicle, $n = 11$; HUCMC, $n = 11$; HVBPs, $n = 10$) by examiners blinded to the experimental groups (two-way analysis of variance [ANOVA], Tukey's multiple comparison post hoc test). **(B–D):** Forelimb motor function was assessed with a grip strength meter **(B)**; whole-body limb function as well as trunk stability was evaluated with the inclined plane test **(C)**; and hind-limb locomotion was assessed by using the 22-point (0–21) Basso, Beattie, and Bresnahan Locomotor Rating Scale **(D)**. At 10 weeks, cross-sectional (30 μm) serial sections ($n = 4$ per group) were stained with Luxol fast blue and H&E and systematically sampled at every 300 μm over a distance of 5,400 μm, and unbiased measurements were made with a Cavalieri probe by using Stereo Investigator. **(E, F):** Representative images at 300 μm rostral to the C7 (35 g) SCI lesion epicenter **(E)** as well as lesional tissue, gray matter, and white matter percent area **(F)** are shown. Data are expressed as percent mean ± SEM. Statistically significant differences between the vehicle control and other conditions are shown in the corresponding experimental group colors, while the differences between HUCMCs and HBVPs are indicated with black asterisks. Two-way ANOVA (Tukey's multiple comparison). *, $p \leq .05$; **, $p \leq .01$; ***, $p \leq .001$; ****, $p \leq .0001$. Abbreviations: BBB, Basso, Beattie, and Bresnahan; HBVPs, human brain vascular pericytes; HUCMCs, human umbilical cord matrix cells; SCI, spinal cord injury.

and tumor necrosis factor-α-stimulated gene 6 (TSG-6) [8]. In 2012, Menge et al. demonstrated that increased levels of circulating human TIMP-3 after human MSC infusion led to preservation of the blood-brain barrier after TBI [6]. They also showed that endogenous TIMP-3 production was significantly increased in the lungs and spleen, which suggests that, despite transient cell engraftment, organs can have an altered inflammatory response [6]. Although we did not measure changes in TIMP-3 here, we found a trend (two-way ANOVA, $p = .07$) toward increased levels of circulating TIMP-1 with cell infusion (HUCMCs and HBVPs).

Alternatively, Watanabe et al. replicated the effects on decreasing blood-brain barrier permeability with systemic administration of TSG-6 [8]. They demonstrated that both treatments reduced neutrophil infiltration at the injury site [8] and implicated this as a potential mechanism of action. Although a significant difference in neutrophils within the spinal cord was not found here (supplemental online Fig. 1), we did detect an increase of rodent IL-10 in plasma (Fig. 3). Despite reports of raised IL-10 levels after stromal cell delivery in various disease models [51–55], systemic changes in IL-10 have not been previously implicated as the primary mechanism by which MSCs lead to neuroprotection.

Systemic IL-10 Is Neuroprotective in SCI

Several studies have evaluated IL-10 in CNS trauma [56]. Brewer et al. demonstrated that intravenous infusion of IL-10 reduced lesion size and neuronal death after SCI [57]. Interestingly, the authors found that intraspinal administration exacerbated the damage [57]. This suggested that IL-10 benefits might uniquely target the systemic response to neurotrauma. Knoblach and Faden confirmed these findings by showing that vascular administration of IL-10 after TBI improved neurological recovery, whereas delivery into the cerebral ventricles had no positive effects [58]. Together, these results are in agreement with our findings, in which increased levels of circulating IL-10 and related vascular effects do not coincide with changes in spinal cord IL-10 levels (Fig. 4). There is also evidence that systemic IL-10 may selectively target endothelial cells [59]. Through inhibition of monocyte adhesion to vasculature, IL-10 can reduce the expression of matrix metalloproteinases (MMPs) and therefore the degradation of the vascular basement membrane. Future work should include assessment of monocyte adhesion and changes in MMP activity. Overall, there is convincing evidence that IL-10 has neuroprotective effects in CNS injuries, highlighting a potential therapeutic mechanism of our cell infusion.

Differences Between HUCMCs and HBVPs

Recognized as major players in CNS trauma [60], pericytes have been discovered to share a common origin [13] with traditionally defined MSCs. This has led to growing interest in pericytes for cell therapy and regenerative medicine [61].

Although HUCMCs and HBVPs had largely similar effects on acute spinal cord pathology, there were notable differences. HBVPs uniquely decreased levels of plasma LIX/CXCL5 and displayed a trend toward raised thymus chemokine (CXCL7, $p = .06$) levels. There was also a trend toward a reduction in circulating RANTES ($p = .06$) and an improvement in functional vascularity at 1 day after SCI.

Moreover, long-term functional recovery was greater with HBVP-infusion. Only HBVPs led to improvements on the inclined

plane test and BBB scores. As a result, it is possible that HBVPs may have other immunomodulatory effects outside of our detection, which would result in improved recovery after SCI. Furthermore, although HBVPs have availability and ethical limitations compared with HUCMCs, advances in induced-pluripotent stem cell technologies may have the potential to create patient-specific cells in the future.

Technical Considerations

The rapid growth in MSC research and the clinical and commercial potential of these cells has led researchers to seek highly specific characteristics/functions from a diverse range of tissues [62]. However, artifacts in isolation procedures, culture conditions, and general cell heterogeneity have limited progress [63]. Our work, which involves cell source comparisons, is susceptible to these limitations. Principally to maintain cell identity, HUCMCs and HBVPs were grown in cell-specific medium. Although this may be a confounding factor [64], we performed extensive antigenic profiling (Fig. 1). Furthermore, all cells were passage-matched at infusion and batch-randomized.

Conclusion

With growing developments in MSC applications, recognizing the optimal cell source for CNS conditions is vital to clinical translation. We show that a minimally invasive intravenous stromal cell transplantation procedure can mitigate secondary pathology. Despite low cell engraftment in the spinal cord, significant systemic changes in inflammatory cytokines occurred after cell infusions, likely facilitated through splenic changes. A significant rise in splenic IL-10 and a trend toward preservation of spleen mass further suggest that this is a major site of cell-mediated immunomodulation. The early protective effects also resulted in enhanced functional recovery and tissue preservation after SCI. Together, these data warrant further study of the splenic role in secondary pathology and cell-based reparative mechanisms for future clinical translation.

Acknowledgments

We thank Ahad Siddiqui and Madeleine O'Higgins for manuscript review and editing and Jian Wang for technical support. This work was supported by funds from the Canadian Institutes of Health Research Training Program in Regenerative Medicine (A.B.) and the Ontario Graduate Scholarship (A.B.). M.F. was supported by the Halbert Chair in Neural Repair and Regeneration and Dezwirek Family Foundation.

Author Contributions

A.B.: conception and design, collection and/or assembly of data, data analysis and interpretation, manuscript writing, final approval of manuscript; R.V.: conception and design, collection and/or assembly of data, data analysis and interpretation, manuscript editing, final approval of manuscript; A.L.: conception and design, collection and/or assembly of data, manuscript editing, final approval of manuscript; J.H.: collection and/or assembly of data, manuscript editing, final approval of manuscript; M.M. and R.D.: collection and/or assembly of data, final approval of manuscript; A.J.: collection and/or assembly of data; M.F: conception and design, data analysis and interpretation, financial support, manuscript editing, final approval of manuscript.

Disclosure of Potential Conflicts of Interest

A.J. had compensated employment as a summer research student. The other authors indicated no potential conflicts of interest.

References

1 Tator CH, Fehlings MG. Review of the secondary injury theory of acute spinal cord trauma with emphasis on vascular mechanisms. J Neurosurg 1991;75:15–26.

2 Rice T, Larsen J, Rivest S et al. Characterization of the early neuroinflammation after spinal cord injury in mice. J Neuropathol Exp Neurol 2007;66:184–195.

3 Schwartz M, Yoles E. Immune-based therapy for spinal cord repair: Autologous macrophages and beyond. J Neurotrauma 2006;23:360–370.

4 De Miguel MP, Fuentes-Julián S, Blázquez-Martínez A et al. Immunosuppressive properties of mesenchymal stem cells: Advances and applications. Curr Mol Med 2012;12:574–591.

5 Aertker BM, Bedi S, Cox CS. Strategies for CNS repair following TBI. Exp Neurol 2016;275:411–426.

6 Menge T, Zhao Y, Zhao J et al. Mesenchymal stem cells regulate blood-brain barrier integrity through TIMP3 release after traumatic brain injury. Sci Transl Med 2012;4:161ra150.

7 Zhang R, Liu Y, Yan K et al. Anti-inflammatory and immunomodulatory mechanisms of mesenchymal stem cell transplantation in experimental traumatic brain injury. J Neuroinflammation 2013;10:106.

8 Watanabe J, Shetty AK, Hattiangady B et al. Administration of TSG-6 improves memory after traumatic brain injury in mice. Neurobiol Dis 2013;59:86–99.

9 Walker PA, Shah SK, Jimenez F et al. Intravenous multipotent adult progenitor cell therapy for traumatic brain injury: Preserving the blood brain barrier via an interaction with splenocytes. Exp Neurol 2010;225:341–352.

10 Matsushita T, Lankford KL, Arroyo EJ et al. Diffuse and persistent blood-spinal cord barrier disruption after contusive spinal cord injury rapidly recovers following intravenous infusion of bone marrow mesenchymal stem cells. Exp Neurol 2015;267:152–164.

11 Walker PA, Bedi SS, Shah SK et al. Intravenous multipotent adult progenitor cell therapy after traumatic brain injury: Modulation of the resident microglia population. J Neuroinflammation 2012;9:228.

12 Bedi SS, Hetz R, Thomas C et al. Intravenous multipotent adult progenitor cell therapy attenuates activated microglial/macrophage response and improves spatial learning after traumatic brain injury. Stem Cells Translational Medicine 2013;2:953–960.

13 Devine SM, Bartholomew AM, Mahmud N et al. Mesenchymal stem cells are capable of homing to the bone marrow of non-human primates following systemic infusion. Exp Hematol 2001;29:244–255.

14 da Silva Meirelles L, Fontes AM, Covas DT et al. Mechanisms involved in the therapeutic properties of mesenchymal stem cells. Cytokine Growth Factor Rev 2009;20:419–427.

15 Liao GP, Harting MT, Hetz RA et al. Autologous bone marrow mononuclear cells reduce therapeutic intensity for severe traumatic brain injury in children. Pediatr Crit Care Med 2015;16:245–255.

16 Oliveri RS, Bello S, Biering-Sørensen F. Mesenchymal stem cells improve locomotor recovery in traumatic spinal cord injury: Systematic review with meta-analyses of rat models. Neurobiol Dis 2014;62:338–353.

17 Alexanian AR, Kwok W-M, Pravdic D et al. Survival of neurally induced mesenchymal cells may determine degree of motor recovery in injured spinal cord rats. Restor Neurol Neurosci 2010;28:761–767.

18 da Silva Meirelles L, Chagastelles PC, Nardi NB. Mesenchymal stem cells reside in virtually all post-natal organs and tissues. J Cell Sci 2006;119:2204–2213.

19 Crisan M, Yap S, Casteilla L et al. A perivascular origin for mesenchymal stem cells in multiple human organs. Cell Stem Cell 2008;3:301–313.

20 da Silva Meirelles L, Caplan AI, Nardi NB. In search of the in vivo identity of mesenchymal stem cells. STEM CELLS 2008;26:2287–2299.

21 Hegyi B, Sági B, Kovács J et al. Identical, similar or different? Learning about immunomodulatory function of mesenchymal stem cells isolated from various mouse tissues: Bone marrow, spleen, thymus and aorta wall. Int Immunol 2010;22:551–559.

22 Ivanova-Todorova E, Bochev I, Mourdjeva M et al. Adipose tissue-derived mesenchymal stem cells are more potent suppressors of dendritic cells differentiation compared to bone marrow-derived mesenchymal stem cells. Immunol Lett 2009;126:37–42.

23 Bochev I, Elmadjian G, Kyurkchiev D et al. Mesenchymal stem cells from human bone marrow or adipose tissue differently modulate mitogen-stimulated B-cell immunoglobulin production in vitro. Cell Biol Int 2008;32:384–393.

24 Williams K, Alvarez X, Lackner AA. Central nervous system perivascular cells are immunoregulatory cells that connect the CNS with the peripheral immune system. Glia 2001;36:156–164.

25 Soubeyrand M, Badner A, Vawda R et al. Very high resolution ultrasound imaging for real-time quantitative visualization of vascular disruption after spinal cord injury. J Neurotrauma 2014;31:1767–1775.

26 Brown A, Nabel A, Oh W et al. Perfusion imaging of spinal cord contusion: Injury-induced blockade and partial reversal by β2-agonist treatment in rats. J Neurosurg Spine 2014;20:164–171.

27 Lee RH, Pulin AA, Seo MJ et al. Intravenous hMSCs improve myocardial infarction in mice because cells embolized in lung are activated to secrete the anti-inflammatory protein TSG-6. Cell Stem Cell 2009;5:54–63.

28 Figley SA, Khosravi R, Legasto JM et al. Characterization of vascular disruption and blood-spinal cord barrier permeability following traumatic spinal cord injury. J Neurotrauma 2014;31:541–552.

29 Warnick RE, Fike JR, Chan PH et al. Measurement of vascular permeability in spinal cord using Evans Blue spectrophotometry and correction for turbidity. J Neurosci Methods 1995;58:167–171.

30 Choudhri TF, Hoh BL, Solomon RA et al. Use of a spectrophotometric hemoglobin assay to objectively quantify intracerebral hemorrhage in mice. Stroke 1997;28:2296–2302.

31 Nguyen DH, Cho N, Satkunendrarajah K et al. Immunoglobulin G (IgG) attenuates neuroinflammation and improves neurobehavioral recovery after cervical spinal cord injury. J Neuroinflammation 2012;9:224.

32 Forgione N, Karadimas SK, Foltz WD et al. Bilateral contusion-compression model of incomplete traumatic cervical spinal cord injury. J Neurotrauma 2014;31:1776–1788.

33 Rivlin AS, Tator CH. Objective clinical assessment of motor function after experimental spinal cord injury in the rat. J Neurosurg 1977; 47:577–581.

34 Basso DM, Beattie MS, Bresnahan JC. A sensitive and reliable locomotor rating scale for open field testing in rats. J Neurotrauma 1995;12:1–21.

35 Chen C-W, Okada M, Proto JD et al. Human pericytes for ischemic heart repair. STEM CELLS 2013;31:305–316.

36 Avolio E, Meloni M, Spencer HL et al. Combined intramyocardial delivery of human pericytes and cardiac stem cells additively improves the healing of mouse infarcted hearts through stimulation of vascular and muscular repair. Circ Res 2015;116:e81–e94.

37 Mendel TA, Clabough EBD, Kao DS et al. Pericytes derived from adipose-derived stem cells protect against retinal vasculopathy. PLoS One 2013;8:e65691.

38 Elenkov IJ, Wilder RL, Chrousos GP et al. The sympathetic nerve—an integrative interface between two supersystems: The brain and the immune system. Pharmacol Rev 2000; 52:595–638.

39 Lucin KM, Sanders VM, Jones TB et al. Impaired antibody synthesis after spinal cord injury is level dependent and is due to sympathetic nervous system dysregulation. Exp Neurol 2007;207:75–84.

40 Fleming JC, Bailey CS, Hundt H et al. Remote inflammatory response in liver is dependent on the segmental level of spinal cord injury. J Trauma Acute Care Surg 2012;72: 1194–1201; discussion 1202.

41 Zhang Y, Guan Z, Reader B et al. Autonomic dysreflexia causes chronic immune suppression after spinal cord injury. J Neurosci 2013;33:12970–12981.

42 Rosas-Ballina M, Ochani M, Parrish WR et al. Splenic nerve is required for cholinergic antiinflammatory pathway control of TNF in endotoxemia. Proc Natl Acad Sci USA 2008; 105:11008–11013.

43 Huston JM, Rosas-Ballina M, Xue X et al. Cholinergic neural signals to the spleen downregulate leukocyte trafficking via CD11b. J Immunol 2009;183:552–559.

44 Acosta SA, Tajiri N, Hoover J et al. Intravenous bone marrow stem cell grafts preferentially migrate to spleen and abrogate chronic inflammation in stroke. Stroke 2015;46:2616–2627.

45 Vendrame M, Gemma C, Pennypacker KR et al. Cord blood rescues stroke-induced changes in splenocyte phenotype and function. Exp Neurol 2006;199:191–200.

46 Tang G, Liu Y, Zhang Z et al. Mesenchymal stem cells maintain blood-brain barrier integrity by inhibiting aquaporin-4 upregulation after cerebral ischemia. STEM CELLS 2014;32:3150–3162.

47 Yu DS, Liu LB, Cao Y et al. Combining bone marrow stromal cells with green tea polyphenols attenuates the blood-spinal cord barrier permeability in rats with compression spinal cord injury. J Mol Neurosci 2015;56:388–396.

48 Chen M, Li X, Zhang X et al. The inhibitory effect of mesenchymal stem cell on blood-brain barrier disruption following intracerebral hemorrhage in rats: Contribution of TSG-6. J Neuroinflammation 2015;12:61.

49 Honma T, Honmou O, Iihoshi S et al. Intravenous infusion of immortalized human mesenchymal stem cells protects against injury in a cerebral ischemia model in adult rat. Exp Neurol 2006;199:56–66.

50 Iihoshi S, Honmou O, Houkin K et al. A therapeutic window for intravenous administration of autologous bone marrow after cerebral ischemia in adult rats. Brain Res 2004;1007:1–9.

51 Burchfield JS, Iwasaki M, Koyanagi M et al. Interleukin-10 from transplanted bone marrow mononuclear cells contributes to cardiac protection after myocardial infarction. Circ Res 2008;103:203–211.

52 Dayan V, Yannarelli G, Billia F et al. Mesenchymal stromal cells mediate a switch to alternatively activated monocytes/macrophages after acute myocardial infarction. Basic Res Cardiol 2011;106:1299–1310.

53 Min C-K, Kim B-G, Park G et al. IL-10-transduced bone marrow mesenchymal stem cells can attenuate the severity of acute graft-versus-host disease after experimental allogeneic stem cell transplantation. Bone Marrow Transplant 2007;39:637–645.

54 Choi J-J, Yoo S-A, Park S-J et al. Mesenchymal stem cells overexpressing interleukin-10 attenuate collagen-induced arthritis in mice. Clin Exp Immunol 2008;153:269–276.

55 Tsumuraya T, Ohtaki H, Song D et al. Human mesenchymal stem/stromal cells suppress spinal inflammation in mice with contribution of pituitary adenylate cyclase-activating polypeptide (PACAP). J Neuroinflammation 2015;12:35.

56 Thompson CD, Zurko JC, Hanna BF et al. The therapeutic role of interleukin-10 after spinal cord injury. J Neurotrauma 2013;30:1311–1324.

57 Brewer KL, Bethea JR, Yezierski RP. Neuroprotective effects of interleukin-10 following excitotoxic spinal cord injury. Exp Neurol 1999; 159:484–493.

58 Knoblach SM, Faden AI. Interleukin-10 improves outcome and alters proinflammatory cytokine expression after experimental traumatic brain injury. Exp Neurol 1998;153: 143–151.

59 Mostafa Mtairag E, Chollet-Martin S, Oudghiri M et al. Effects of interleukin-10 on monocyte/endothelial cell adhesion and MMP-9/TIMP-1 secretion. Cardiovasc Res 2001;49: 882–890.

60 Göritz C, Dias DO, Tomilin N et al. A pericyte origin of spinal cord scar tissue. Science 2011;333:238–242.

61 Birbrair A, Zhang T, Wang Z-M et al. Pericytes at the intersection between tissue regeneration and pathology. Clin Sci (Lond) 2015;128: 81–93.

62 Keating A. Mesenchymal stromal cells: New directions. Cell Stem Cell 2012;10:709–716.

63 Lv F-J, Tuan RS, Cheung KMC et al. Concise review: The surface markers and identity of human mesenchymal stem cells. STEM CELLS 2014;32:1408–1419.

64 Blocki A, Wang Y, Koch M et al. Not all MSCs can act as pericytes: Functional in vitro assays to distinguish pericytes from other mesenchymal stem cells in angiogenesis. Stem Cells Dev 2013;22:2347–2355.

See www.StemCellsTM.com for supporting information available online.

